A key role of tensile strain and surface termination in formation and properties of $La_{0.7}Sr_{0.3}MnO_3$ composites with carbon nanotubes

Evgenia A. Kovaleva[1*], Alexander A. Kuzubov[1,2], Pavel V. Avramov[3], Anastasia S. Kholtobina[1], Artem V. Kuklin[1,3], Felix N. Tomilin[1,2], Pavel B. Sorokin[4]

[1]Siberian Federal University, 79 Svobodny pr., Krasnoyarsk, 660041,Russia

[2]L.V. Kirensky Institute of Physics, 50 Akademgorodok, Krasnoyarsk, 660036,Russia

[3]Kyungpook National University, 80 Daehakro, Bukgu, Daegu, 41566, Korea

[4]National University of Science and Technology MISiS, 4 Leninskiy prospekt, Moscow 119049, Russian Federation

Abstract

Atomic and electronic structure of LSMO-based composites with carbon nanotubes were studied by means of density functional theory with respect to the termination of LSMO surface. The deformation of the tubes caused by the lattice mismatch with the substrate leads to a major change in their electronic structure. The surface terminated with Mn-O layer provides much stronger interaction with carbon nanotubes than Sr-O terminated one does. The interaction with transition metal atoms is essential for spin polarization of the nanotube while no spin injection was observed for Sr-O-supported tubes.

Keywords: carbon nanotubes, LSMO, interface, spin polarization

[*]tel.: +7(923)2764752, fax.: +7(391)2062109, e-mail: kovaleva.evgeniya1991@mail.ru

1. Introduction

Half-metallic $La_{0.7}Sr_{0.3}MnO_3$ (LSMO) is widely used in spintronic and spincaloritronic devices due to its unique properties like half-metallic nature and high Curie temperature (T_c=370K, the highest among substituted lanthanum manganites) [1–5]. Nanosized materials are of particular interest since their usage allows one to significantly increase the efficiency of the devices. Moreover, material's properties can be altered drastically when turning from the bulk material to a nanostate [6] since the high surface area along with structural defects leads to the increasing influence of morphology and grain boundaries in comparison with conventional form of LSMO [7].

Recently the composites of LSMO with various carbon nanostructures such as fullerenes, graphene zig-zag nanoribbons and multiwall CNTs were studied by several scientific groups [8–12]. $La_{0.8}Sr_{0.2}MnO_3$ nanoparticle-decorated carbon nanotubes demonstrate metal-insulator transition and paramagnetic to superparamagnetic phase transition both rising from the presence of LSMO nanoparticles [8]. Anisotropic nature of magnetic field-magnetization curve and high coercivity allows one to use carbon nanotubes fabricated on the $La_{0.66}Sr_{0.33}MnO_3$ as constituting fragments of spintronic nanodevices [9]. Another application of LSMO/CNT composites is electrocatalysis, since they can act as cathode catalysts for oxygen reduction [10].

It was found that exchange interaction with LSMO support causes large spin polarization of graphene zig-zag nanoribbons, whereas carbon nanotubes remain to be slightly spin-polarized. Devices of multiwall carbon nanotube between two half-metallic LSMO electrodes demonstrate electric conductance increasing at lower temperatures [11] along with high spin polarization of electrodes and the resistance for spin injection [12]. These experimental results were also supported by density functional theory calculations.

The special kind of magnetic ordering in C_{60} molecule rising from the interaction with manganese atoms was found to be responsible for binding between fullerene and LSMO and complex magnetic exchange interaction [13]. One can speculate that binding with manganese should affect electronic structure of carbon nanotubes deposited on LSMO surface as well. Previous studies of zigzag and armchair CNTs deposited on ferromagnetic substrates demonstrated their significant spin polarization due to the interaction with 3d metals [14,15]. One could expect even higher values of spin polarization for CNT caused by interactions with half-metallic material. The main goal of this study is to reveal the role of both Mn and Sr ions in determination of the spin-related properties of LSMO-based heterostructures.

2. Computational methods

The first-principles density functional theory calculations of LSMO/CNT composites were performed using VASP code [16–19]. GGA PBE functional [20,21] with taking into account Hubbard corrections (GGA+U) [22,23] and projector augmented wave [24,25] method (PAW) were implemented . D3 Grimme correction of weak dispersion interactions [26] was used in order to describe the interaction between nanotubes and LSMO substrate correctly. The U=2 and J=0.7 eV parameters for Mn atoms were adopted from earlier calculations of LSMO and carefully tested with respect to the lattice parameters and electronic properties of both bulk and slab LSMO [27–29]. Full geometry optimization was performed until the forces acting on atoms were less than 0.01 eV/Å.

First, the unit cell of bulk LSMO was optimized, and the *a* translation vector is found to be equal to 3.886 Å which is in a good agreement with experimental data (*a*=3.876 Å [30] and *a*=3.87 Å [31]) and previous theoretical calculations (*a*=3.89 Å) [27]. Then, LSMO(001) surface was constructed by cutting it along the

corresponding crystallographic plane. Both bulk LSMO and the corresponding slab were found to be half-metallic, in agreement with TMR and photoemission spectroscopy data [32,33].

Depending on the synthesis conditions, the slab of LSMO can be terminated by either Sr-O or Mn-O layer (see Figure 1). We suppose it's worth considering both surfaces since, as was shown in our previous study of LSMO/C_{60} composites [13], the interaction between carbon conjugated structure and transition metal atoms is crucial for the formation of composite and responsible for its properties. Thus, one can expect much stronger interaction with Mn-O terminated surface and only a weak van-der-Waals interaction with Sr-O terminated one.

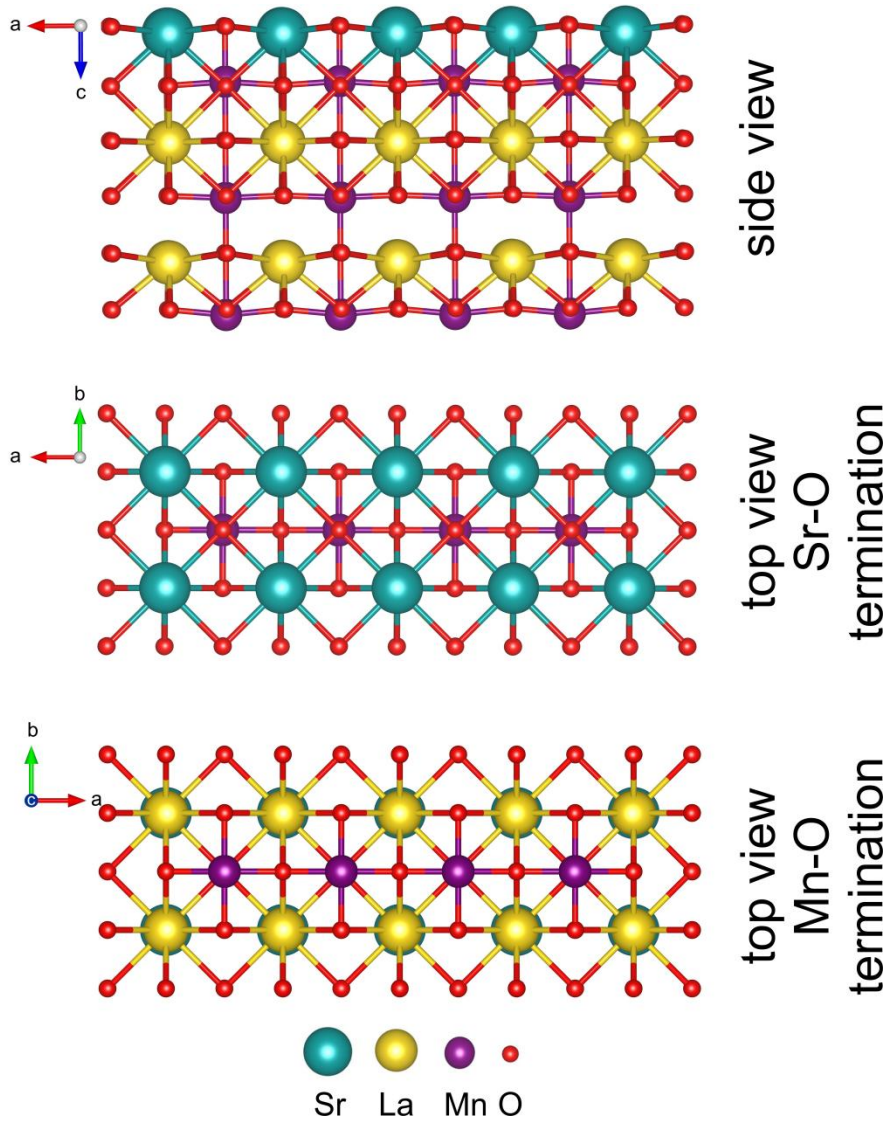

Figure 1. Top and side views of Mn-O and Sr-O terminated LSMO slab

Two different supercells of LSMO slab were used: 8×1 (*a*=31.09 Å, *b*=3.88 Å) for CNT(9,0) and 6×2 (*a*= 23.32 Å, *b*=7.77 Å) for CNT(5,5). However, CNT(9,0) was still contracted by ~9% and CNT(5,5) was stretched by ~5% which changes their properties significantly (see Section 3.1). Neighbouring nanotubes must be located as far as possible from each other, so LSMO slabs consisted of 8 and 6 unit cells, respectively, in direction normal to the tube's axis, which were the minimum values for providing both correct description and computational efficiency. We suppose that mainly the topmost layer should be responsible for the interface properties so one can use an oversimplified model of 1 unit cell along *c* direction (the thickness of the slab is then 9.81 Å) without any cost at computational accuracy while considerably increasing the speed of calculations [34,35]. Artificial interactions in periodic boundary conditions were avoided by setting the vacuum interval in direction normal to the interface so the *c* translation vector was equal to 30 Å. The Mönkhorst-Pack [36] k-point Brilloin sampling was used. The k-point grid contained 1×6×1 and 1×2×1 points along *a*, *b* and *c* directions for different supercells, respectively. The energy cut-off was specified as 450 eV in all calculations.

Energy of bonding between nanotubes and LSMO slab was estimated as:

$$E_b = E_c - E_{NT} - E_{LSMO}, \quad (1)$$

where E_c, E_{NT} and E_{LSMO} are total energies of composite, nanotube and LSMO slab, respectively. Charges and magnetic moments were estimated according to the Bader charge analysis [31–33].

3. Results and Discussion

3.1. Interaction with Sr-O terminated surface

Three CNT(9,0)/LSMO(Sr-O) configurations (Figure 2) were considered. The first Sr(η^2) configuration (Sr ion coordinated to C-C bond) is presented in Figure 2a. The second Sr(η^3) configuration was originally characterized by Sr ion coordinated to carbon hexagon but was slightly displaced during the optimization resulting in coordination to C_3 fragment of CNT(9,0) (Figure 2b). The third CNT(9,0) O($\eta^{6\text{-}2}$) configuration with two oxygen ions coordinated to η^6 and η^2 positions, respectively, is presented in Figure 2c. As it was previously mentioned, the difference between lattice parameter of LSMO and CNT(9,0) along *a* direction is quite large and results in 9% contraction of the CNT(9,0).

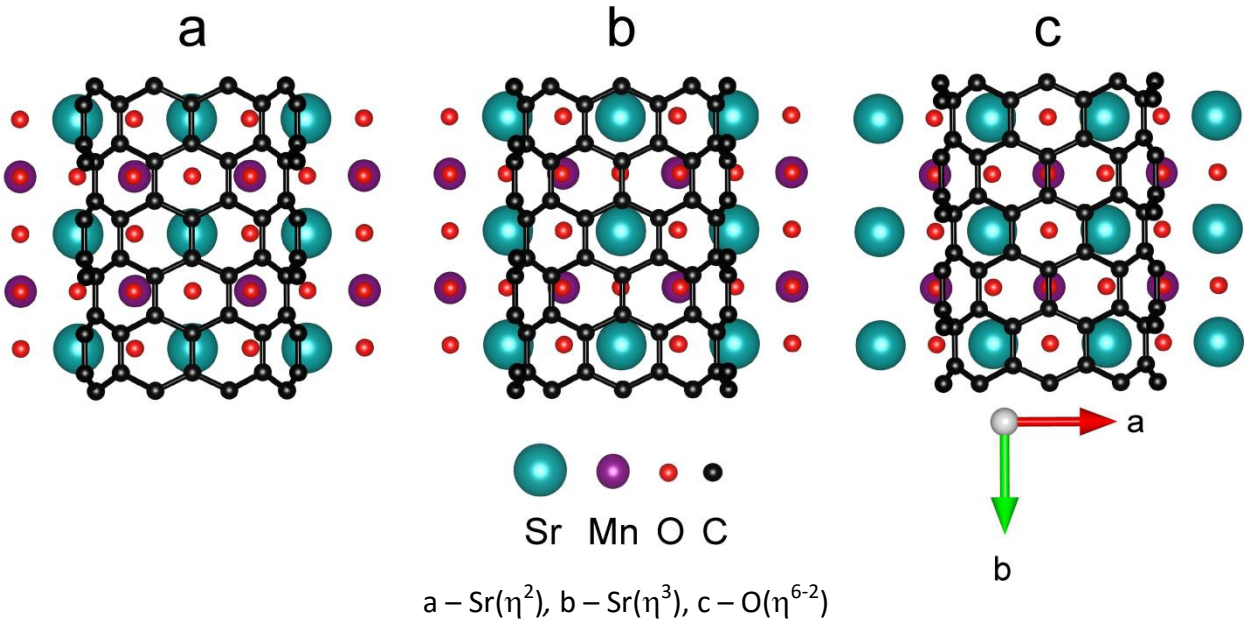

Figure 2. Different configurations of CNT(9,0)/LSMO(Sr-O) nanocomposites. For the sake of better representation, the upper part of tubes is cut.

Similarly to the interfaces of CNTs with ferromagnetic substrates of Co(0001) and Ni(111) [14,15], armchair (5,5) carbon nanotube being very close in diameter to CNT(9,0) (6,97 and 7,05 Å, respectively) was also considered. Since CNT(5,5) and CNT(9,0) have close diameters, the Sr($\eta^{6\text{-}2}$) configuration (Figure 3) was considered for CNT(5,5)/LSMO(Sr-O) heterostructure following the energetic stability of Sr(η^6) configuration of CNT(9,0)/LSMO(Sr-O). The CNT (5,5) slab is stretched by 5% because of mismatch with the structural parameters of LSMO.

The binding energies and shortest bond lengths between CNT and LSMO fragments for CNT-based heterostructures are presented in Table 1.

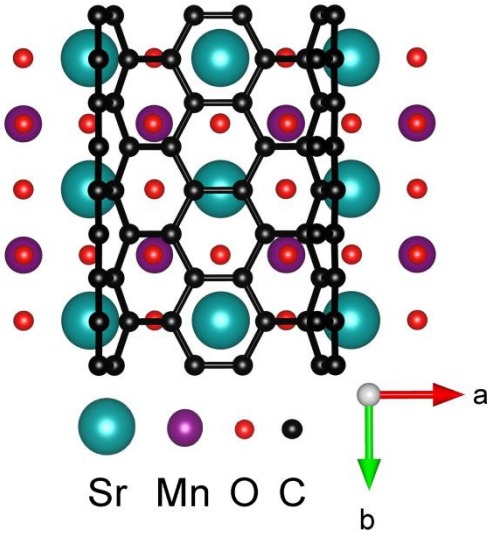

Figure 3. Structure of CNT(5,5)/LSMO(Sr-O) nanocomposite. For the sake of better representation, the upper part of the tube is cut.

Table 1. Binding energies and bond lengths of CNT(9,0)/LSMO(Sr-O) and CNT(5,5)/LSMO(Sr-O) heterostructures

Composite	CNT(9,0)/LSMO			CNT(5,5)/LSMO
	$Sr(\eta^3)$	$O(\eta^{6-2})$	$Sr(\eta^2)$	
Binding energy, eV	-0.5663	-0.3468	1.0213	-2.0710
Bond distance, Å	2.830	3.023	2.898	3.123

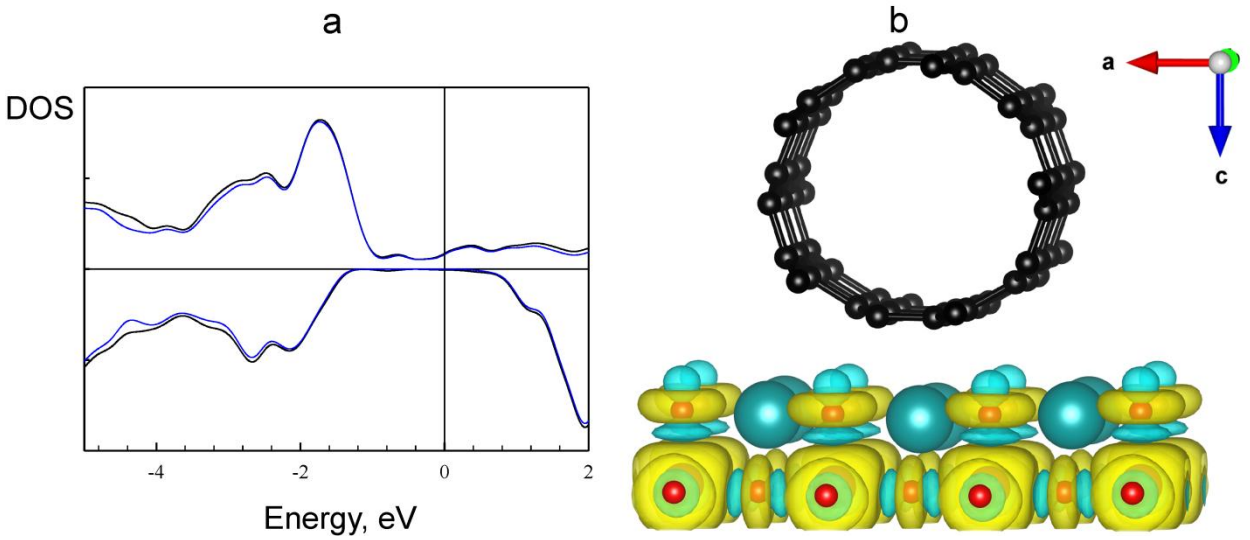

Figure 4. a) Density of states of CNT(9,0)/LSMO(Sr-O) heterostructure. Black and blue lines correspond to the total and partial LSMO DOSes, respectively. b) Spatial distribution of spin density in CNT(5,5)/LSMO(Sr-O) heterostructure. Yellow and blue areas correspond to spin-up and spin-down density, respectively.

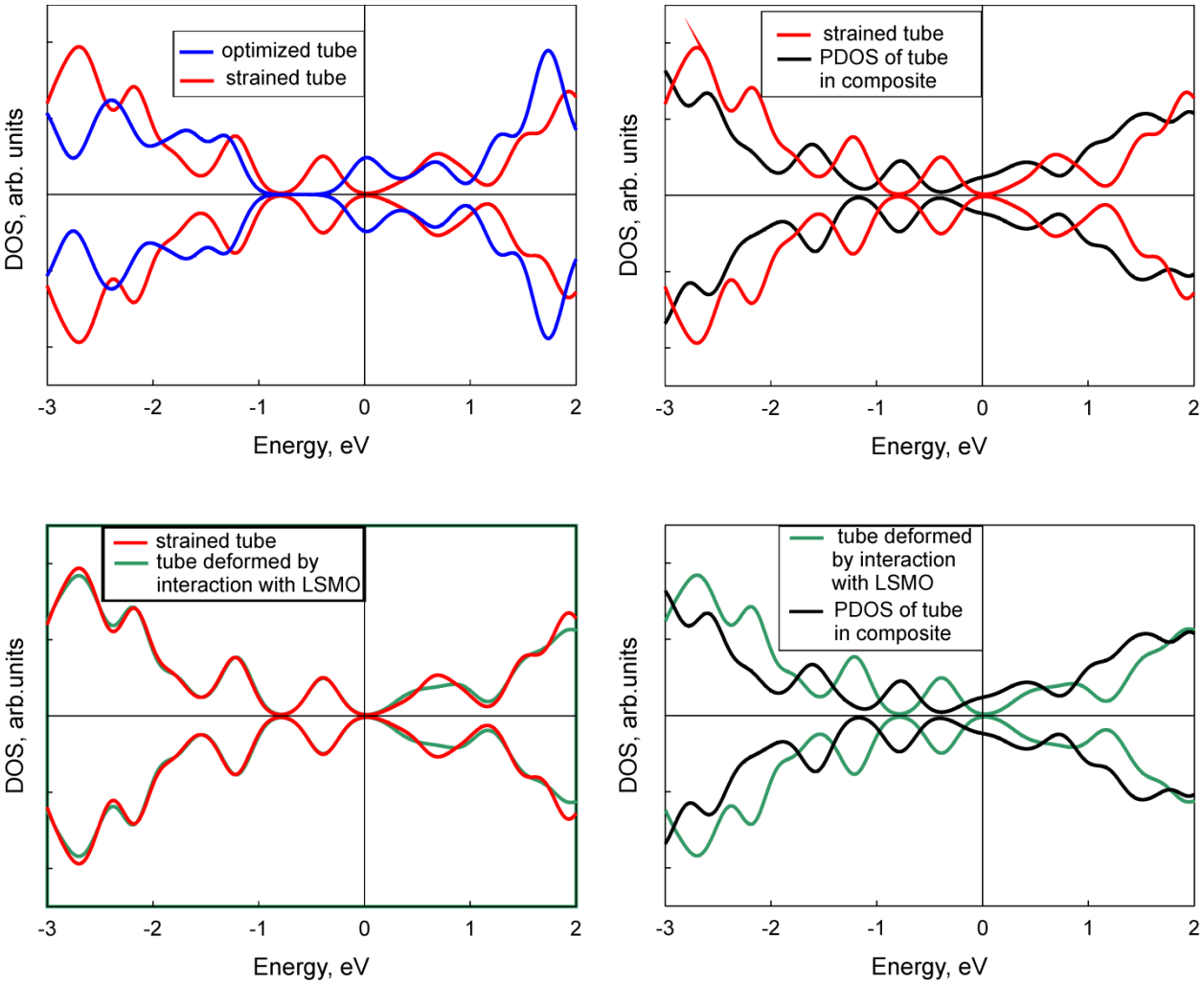

Figure 5. Densities of states for CNT(9,0) Blue, red, green and black lines correspond to the relaxed CNT's structure, strained CNT structure with LSMO translation vector adopted, freestanding CNT at the same geometry as in the composite, and partial density of states the nanotube in CNT/LSMO(Sr-O) composite, respectively.

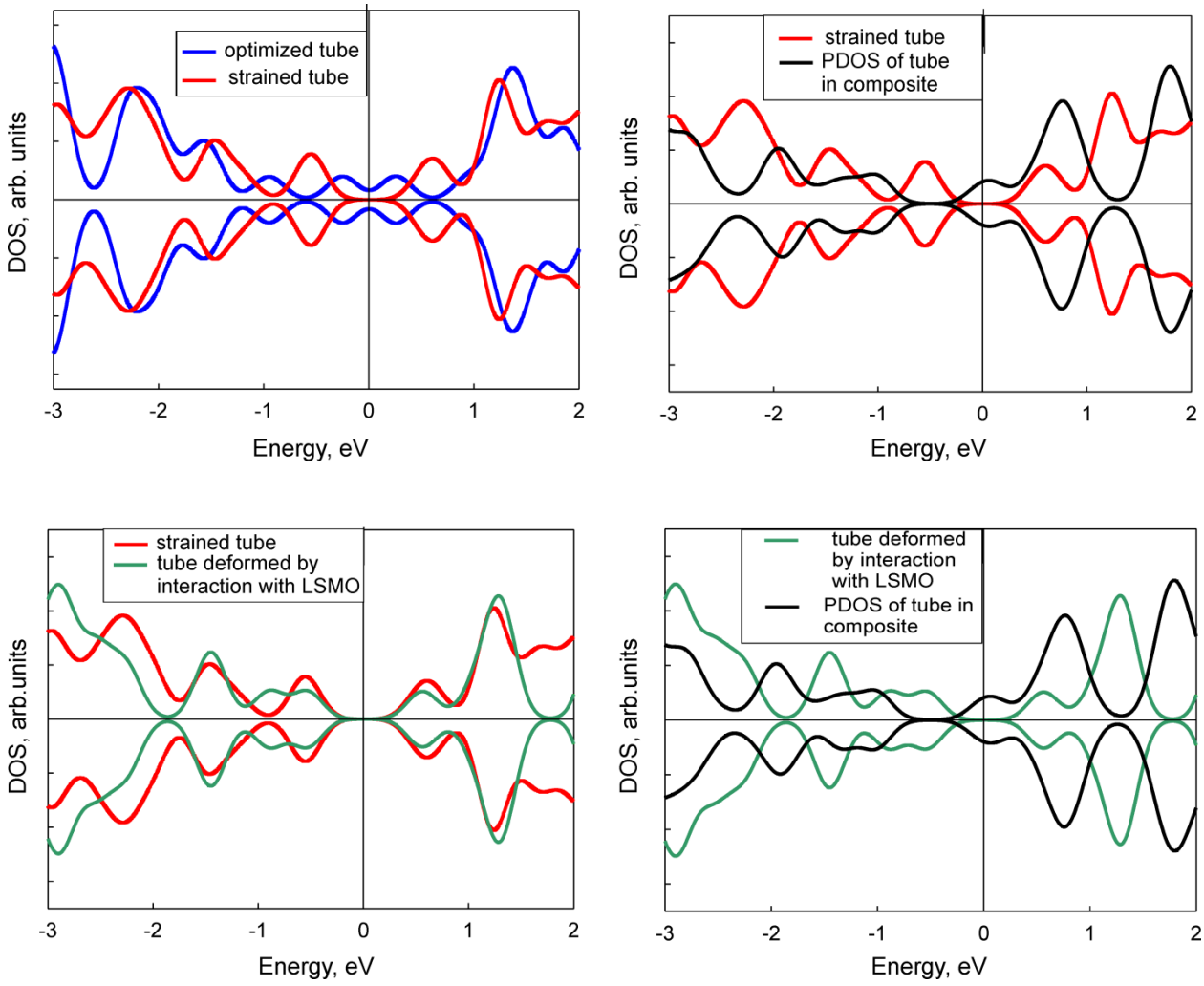

Figure 6. Densities of states for CNT(5,5) Blue, red, green and black lines correspond to the relaxed CNT's structure, strained CNT structure with LSMO translation vector adopted, freestanding CNT at the same geometry as in the composite, and partial density of states the nanotube in CNT/LSMO(Sr-O) composite, respectively.

Values of binding energies and bond distances witness the presence of van der Waals interactions between CNTs and LSMO slab (Table 1). Sr(η^3) configuration is energetically favorable among three CNT(9,0)/LSMO(Sr-O) composites with -0.5663 eV binding energy per supercell (which corresponds to -0.016 eV/carbon

atom). Strontium atom is displaced from the center of carbon hexagon to attain the η^3 site changing Sr(η^6) configuration to Sr(η^3), so the bond length becomes shorter (see Figure 2b). However, Sr(η^2) configuration with comparable bond distance is not stable because of positive binding energy (1.0213 eV or 0.028 eV per carbon atom).

The Sr($\eta^{6\text{-}2}$) configuration of CNT(5,5)/LSMO(Sr-O) heterostructure demonstrates lower binding energy (-2.0710 eV per unit cell or -0.035 eV per carbon atom). No displacement was observed for this configuration.

Since CNT(9,0) and CNT(5,5) have almost the same diameters and they do not create strong covalent bonds with LSMO support, the visible differences in the binding energies of the nanotubes with the LSMO support can be caused by different types and values of structural stress caused by crystal lattice mismatch.

The analysis of composites' electronic structure (Figure 4) shows that it remains almost the same as for the bare LSMO in both cases. Although composites are almost totally spin polarized, it can be seen that this is due to LSMO slab while nanotubes' spin-up and spin-down partial densities of states are of an equal intensity (spin polarization values are ~1.7% and ~0.3% for CNT(5,5) and CNT(9,0), respectively, the absence of visible spin polarization is also confirmed by the spatial spin density distribution).

To study the influence of the associated strain, the free-standing relaxed and stretched (the same stress as for CNTs on LSMO) CNT(9,0) and CNT(5,5) were chosen for the calculations. It should be noticed that stretching and contraction of bare nanotubes leads to the rearrangement of electron density, then unoccupied bands are filled and the Fermi level changes (Figure 5, 6). Similar effect is observed when they interact with LSMO. The strain leads to appearance of a narrow band gap (0.2 eV) and significant shift of the Fermi level in the DOS of CNT(5,5) (Figure 6). Interaction of CNT(5,5) with LSMO fragment leads to the

visible redistribution of peak intensities of the DOS with low spin polarization at Fermi level (1.7%). The same effects are detected for CNT(9,0) as well. The contraction leads to the visible shift of Fermi level, and interaction with LSMO causes further shift and smearing of the peaks. The spin polarization of the CNT(9,0) is even smaller than for CNT(5,5) and is equal to 0.3%. The Bader charge analysis [37–39] shows that total tube charges are equal to 0.4 and 0.8 electron charges for CNT(9,0)/LSMO and CNT(5,5)/LSMO, respectively. In order to shed the light on the nature of peaks shift and smearing when interacting with the substrate, single point calculation was performed for the freestanding nanotubes fixed at the composite geometry. Visible lateral and normal distortion of the tubes in comparison with their initial structure, though being either contracted or stretched (see Figure 4), leads to the abovementioned smearing of the peaks. Densities of states of these structures are very similar to the PDOS of tubes in the composite. However, it can be clearly seen that interaction with the substrate shifts them to the lower energies. Hence, there is considerable interaction between the nanotubes and LSMO slab leading to the changes in their electronic structure. However, most of these changes can still be attributed to the CNTs deformation. Even though the substrate changes the electronic structure of the nanotubes significantly, there is no difference between spin-up and spin-down density, in contrast to ferromagnetic Co(0001) and Ni(111) surfaces [14,15]. The electronic structure of LSMO is also virtually the same as for pristine slab confirming the presence of van-der-Waals interaction between Sr-O terminated LSMO and carbon nanotubes.

3.2. Interaction with Mn-O terminated surface

To study the effects of structural deformation caused by Mn-O terminated surface on the electronic structure of CNT(5,5), a 6×2×1 supercell (a= 23.32 Å, b=7.77 Å, c=30.00 Å) of LSMO slab was used with 1×2×1 k-points along a, b and c

direction. Three configurations of CNT(5,5)/LSMO(Mn-O) composite (Figure 6) were considered, namely, Mn(η^{6-2}) with Mn atoms coordinated to carbon hexagon and C-C bond (Figure 7a); O(η^4) with oxygen atom being slightly displaced from the center of hexagon (Figure 7b); and O(η^{6-2}) configuration with oxygen atoms coordinated to η^6 and η^2 positions (Figure 7c).

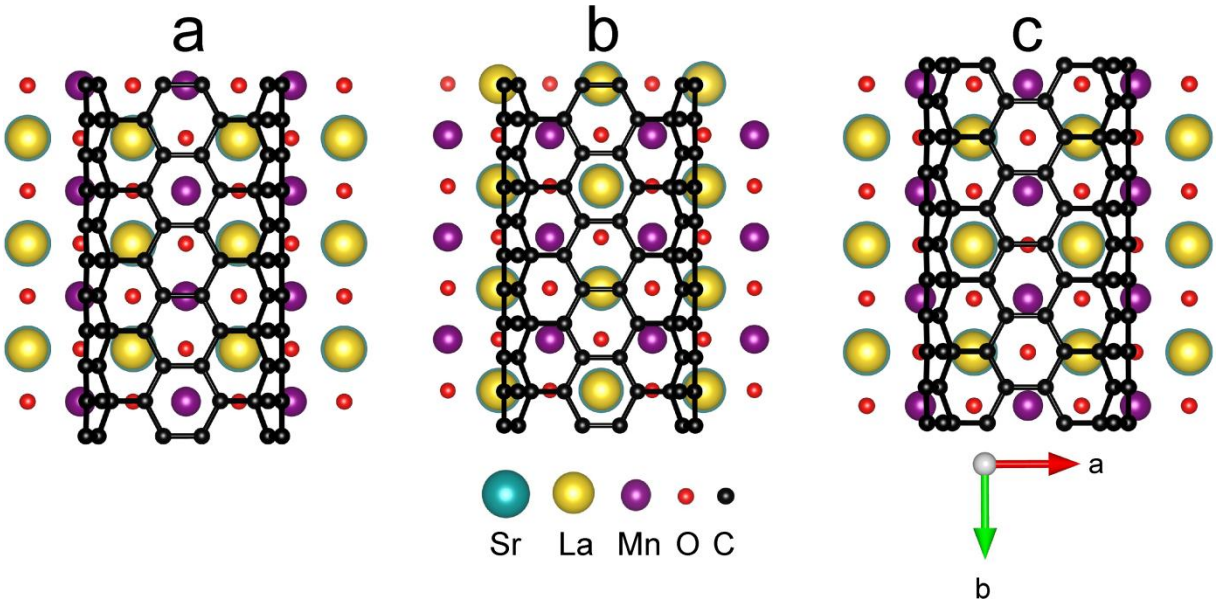

a – Mn(η^{6-2}), b – O(η^4), c – O(η^{6-2})

Figure 7. a) Mn(η^{6-2}), b) O(η^4) and O(η^{6-2}) CNT(5,5)/LSMO(Mn-O) configurations. For the sake of better representation, the upper part of the tube was cut.

The calculations revealed O(η^4) configuration as energetically favorable (Table 2) even though it demonstrates larger bond distance in comparison with Mn(η^{6-2}) and O(η^{6-2}) ones. This may be explained in terms of stronger interactions between nanotube carbon π-system and manganese ions (see Figure 7 and Figure 8). The contact area is mainly presented by the hexagons parallel to the tube axis. Both Mn(η^{6-2}) and O(η^{6-2}) composites are characterized by carbon bonds above the Mn atom. Mn(η^{6-2}) has 2 carbon atoms bonded to one Mn per unit cell, and O(η^{6-2}) has 4 carbon atoms bonded to two manganese atoms. In contrast to that, the unit cell of O(η^4) has 4 carbon atoms bonded to 4 manganese atoms. Moreover, not only unstrained hexagons in direct contact with substrate are involved into

the interaction with the slab, but the hexagons next to them are still affected by the substrate. It can be seen from Figure 7 that there is no overlapping of these hexagons with Mn atoms for Mn(η^{6-2}) and O(η^{6-2}), in contrast to O(η^4) configuration. Each manganese atom in contact area is then coordinated by two carbon hexagons enhancing the bonding between LSMO slab and the nanotube.

The patterns of spin density distribution (Figure 8) support this suggestion: one can see a negative spin polarization of carbon atoms mostly affected by manganese and positive spin polarizations of the atoms next to them, which is very similar to what was observed for buckminsterfullerene deposited on Mn-O terminated LSMO surface [13].

Table 2. Properties of CNT(5,5)/LSMO(Mn-O) nanocomposite

Composite configuration	CNT(5,5)/LSMO		
	Mn(η^{6-2})	O(η^4)	O(η^{6-2})
Binding energy, eV	-1,25	-1,41	-1,23
Bond distance, Å	2,53	2,70	2,65
Charge of the tube, e	0,25	0,28	0,24
Magnetic moment of the tube, μ_B	0,15	0,12	0,13
Spin polarization of the tube at the Fermi level, %	-12,8	-44,2	-12,6

O(η^4) configuration possesses slightly larger charge being transferred to the tube and much larger spin polarization at the Fermi level, in contrast to both Sr-O

terminated surface and other two configurations (see Table 2). The magnetic moment on the tube is, however, slightly smaller than others. This is obviously caused by the effect mentioned above: there are both positively and negatively spin-polarized carbon atoms, and the stronger the interaction between manganese and carbon atoms, the more prominent magnetic ordering, which was previously found for carbon nanostructures on LSMO(Mn-O) surface [13]. Since the O(η^4) is the most symmetric configuration with respect to the Mn ions, positive and negative spin polarization partially compensate each other. However, one could have noticed that binding energy for the CNT(5,5) on LSMO(Mn-O) surface are by ~0.66 eV smaller than that for CNT(5,5) on LSMO(Sr-O) surface even though the interactions between composite fragments are stronger in the former case. This is mainly caused by the major deformation of the tubes when forming these composites (see Figure 8). The energy of nanotube's deformation was estimated to vary from 0.4 to 0.5 depending on the configuration, and, thus, was supposed to be responsible for the difference in binding energy.

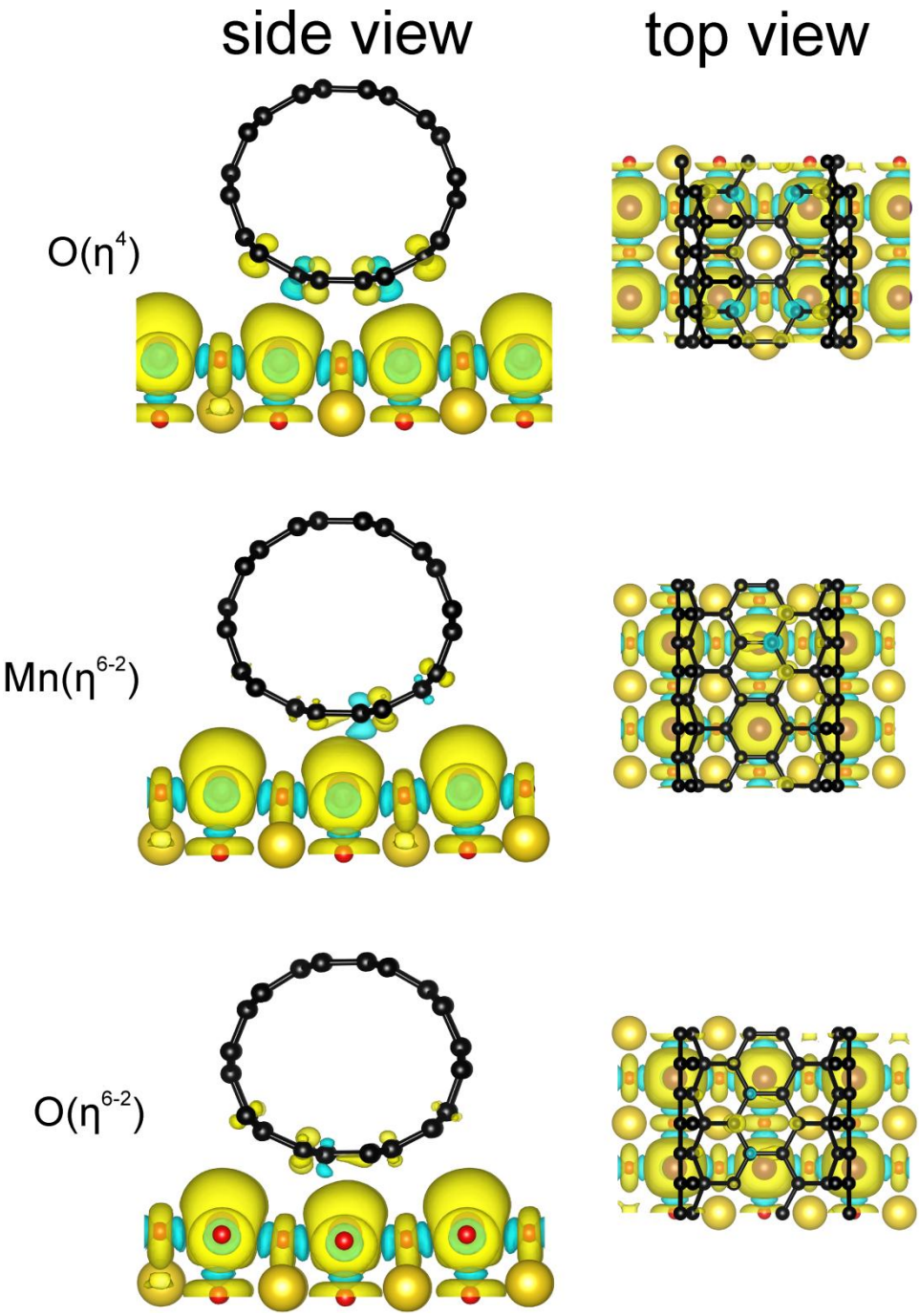

Figure 7. Spatial spin density distribution in CNT(5,5)/LSMO(Mn-O) nanocomposites. Yellow and blue areas correspond to spin-up and spin-down density, respectively.

4. Conclusions

It was found that regardless major deformations of carbon nanotubes atomic structures caused by lattice mismatch with LSMO substrate, the formation of CNT(9,0)/LSMO and CNT(5,5)/LSMO heterostructures is energetically favorable. The interactions of CNT(9,0) and CNT(5,5) with LSMO(Sr-O) slab change noticeably

the electronic structure of the carbon nanotubes mainly due to the structural deformations caused by lattice mismatch. The van-der-Waals interactions are responsible for CNT and LSMO fragments binding, which keeps the LSMO fragment electronic subsystem intact. In contrast to the Sr-O terminated surface, electronic structure calculations reveal visible interactions between CNT(5,5) and Mn-O terminated LSMO. Overlapping between carbon and manganese atoms electronic states plays a key role in composite formation, in agreement with the results obtained for C_{60} [13].

Acknowledgements

This work was supported by National Research Foundation of Republic of Korea under grant No. 2017040381 and the government contract of the Ministry of Education and Science of the Russian Federation to Siberian Federal University (Grant No. 16.1455.2017/PCh). The authors would like to thank Joint Supercomputer Center of RAS, Moscow; Center of Equipment for Joint Use of Siberian Federal University, Krasnoyarsk; and Information Technology Centre, Novosibirsk State University for providing the access to their supercomputers. P.B.S gratefully acknowledges the financial supports of the Ministry of Education and Science of the Russian Federation in the framework of Increase Competitiveness Program of NUST «MISiS» (No. К2-2017-001) and RFBR, according to the research project No. 16-32-60138 mol_a_dk. E.A. Kovaleva would also like to acknowledge the program of the President of Russian Federation for Leading Scientific Schools Support (Grant No. 2016 NSh-7559.2016.2).

References

[1] C. Barraud, P. Seneor, R. Mattana, S. Fusil, K. Bouzehouane, C. Deranlot, P. Graziosi, L. Hueso, I. Bergenti, V. Dediu, F. Petroff, A. Fert, Nat. Phys. 6 (2010) 615–620.

[2] F. Li, T. Li, F. Chen, F. Zhang, Sci. Rep. 5 (2015) 9355.

[3] F. Li, ACS Appl. Mater. Interfaces 5 (2013) 8099–104.

[4] R. Lin, F. Wang, M. Wohlgenannt, C. He, X. Zhai, Y. Suzuki, Synth. Met. 161 (2011) 553–557.

[5] S. Liang, R. Geng, B. Yang, W. Zhao, R. Chandra Subedi, X. Li, X. Han, T.D. Nguyen, Sci. Rep. 6 (2016) 19461.

[6] N. Banerjee, S.B. Krupanidhi, Appl. Phys. A Mater. Sci. Process. 111 (2013) 605–612.

[7] J. Curiale, R.D. Sánchez, H.E. Troiani, A.G. Leyva, P. Levy, Appl. Surf. Sci. 254 (2007) 368–370.

[8] L. Kyu Won, L. Cheol Eui, G. A., S. E., K. Yu., J. Korean Phys. Soc. 59 (2011) 3309.

[9] S.C. Ray, H.M. Tsai, H.C. Chen, S.L. Wu, D.C. Ling, I.N. Lin, W.F. Pong, J Nanosci Nanotechnol 11 (2011) 10710–10714.

[10] K. Miyazaki, K. Kawakita, T. Abe, T. Fukutsuka, K. Kojima, Z. Ogumi, J. Mater. Chem. 21 (2011) 1913.

[11] L.E. Hueso, G. Burnell, J.L. Prieto, L. Granja, C. Bell, D.J. Kang, M. Chhowalla, S.N. Cha, J.E. Jang, G.A.J. Amaratunga, N.D. Mathur, Appl. Phys. Lett. 88 (2006) 6–8.

[12] L.E. Hueso, J.M. Pruneda, V. Ferrari, G. Burnell, J.P. Valdés-Herrera, B.D. Simons, P.B. Littlewood, E. Artacho, A. Fert, N.D. Mathur, Nature 445 (2007) 410–413.

[13] E.A. Kovaleva, A.A. Kuzubov, P.V. Avramov, A.V. Kuklin, N.S. Mikhaleva, P.O. Krasnov, Org. Electron. 37 (2016) 55–60.

[14] A.A. Kuzubov, E.A. Kovaleva, P. Avramov, A. V. Kuklin, N.S. Mikhaleva, F.N. Tomilin, S. Sakai, S. Entani, Y. Matsumoto, H. Naramoto, J. Appl. Phys. 116 (2014).

[15] A.A. Kuzubov, E.A. Kovaleva, F.N. Tomilin, N.S. Mikhaleva, A. V. Kuklin, J. Magn. Magn.

Mater. 396 (2015) 102–105.

[16] G. Kresse, J. Furthmüller, Phys. Rev. B 54 (1996) 11169–11186.

[17] G. Kresse, J. Furthmüller, Comput. Mater. Sci. 6 (1996) 15–50.

[18] G. Kresse, J. Hafner, Phys. Rev. B 49 (1994) 14251–14269.

[19] G. Kresse, J. Hafner, Phys. Rev. B 47 (1993) 558–561.

[20] J.P. Perdew, J.A. Chevary, S.H. Vosko, K.A. Jackson, M.R. Pederson, D.J. Singh, C. Fiolhais, Phys. Rev. B 46 (1992) 6671–6687.

[21] J.P. Perdew, J.A. Chevary, S.H. Vosko, K.A. Jackson, M.R. Pederson, D.J. Singh, C. Fiolhais, Phys. Rev. B 48 (1993) 4978–4978.

[22] V.I. Anisimov, J. Zaanen, O.K. Andersen, Phys. Rev. B 44 (1991) 943–954.

[23] S.L. Dudarev, G.A. Botton, S.Y. Savrasov, C.J. Humphreys, A.P. Sutton, Phys. Rev. B 57 (1998) 1505–1509.

[24] P.E. Blöchl, Phys. Rev. B 50 (1994) 17953–17979.

[25] G. Kresse, D. Joubert, Phys. Rev. B 59 (1999) 1758–1775.

[26] S. Grimme, J. Comput. Chem. 27 (2006) 1787–1799.

[27] C. Ma, Z. Yang, S. Picozzi, J. Phys. Condens. Matter 18 (2006) 7717–28.

[28] S. Picozzi, C. Ma, Z. Yang, R. Bertacco, M. Cantoni, A. Cattoni, D. Petti, S. Brivio, F. Ciccacci, Phys. Rev. B 75 (2007) 94418.

[29] B. Zheng, N. Binggeli, Phys. Rev. B 82 (2010) 245311.

[30] M.C. Martin, G. Shirane, Y. Endoh, K. Hirota, Y. Moritomo, Y. Tokura, Phys. Rev. B 53 (1996) 14285–14290.

[31] F. Tsui, M.C. Smoak, T.K. Nath, C.B. Eom, Appl. Phys. Lett. 76 (2000) 2421.

[32] M. Bowen, M. Bibes, A. Barthélémy, J.-P. Contour, A. Anane, Y. Lemaître, A. Fert, Appl. Phys. Lett. 82 (2003) 233–235.

[33] J.-H. Park, E. Vescovo, H.-J. Kim, C. Kwon, R. Ramesh, T. Venkatesan, Nature 392 (1998)

794–796.

[34] P. Avramov, A.A. Kuzubov, A. V. Kuklin, H. Lee, E.A. Kovaleva, S. Sakai, S. Entani, H. Naramoto, P.B. Sorokin, J. Phys. Chem. A 121 (2017) 680–689.

[35] A. V. Kuklin, A.A. Kuzubov, E.A. Kovaleva, H. Lee, P.B. Sorokin, S. Sakai, S. Entani, H. Naramoto, P. Avramov, J. Magn. Magn. Mater. (2016).

[36] H.J. Monkhorst, J.D. Pack, Phys. Rev. B 13 (1976) 5188–5192.

[37] W. Tang, E. Sanville, G. Henkelman, J. Phys. Condens. Matter 21 (2009) 84204.

[38] E. Sanville, S.D. Kenny, R. Smith, G. Henkelman, J. Comput. Chem. 28 (2007) 899–908.

[39] G. Henkelman, A. Arnaldsson, H. Jónsson, Comput. Mater. Sci. (2006).